

Theory-guided Investigation on Magnetic Evolution of $\text{MnPt}_{5-x}\text{Pd}_x\text{P}$ and Discovery of anti-CeCoIn₅-type Ferromagnetic MnPd_5P

Ranuri S. Dissanayaka Mudiyansele,¹ Chang-Jong Kang,^{2,3} Kaya Wei,⁴ Zhixue Shu⁵, Tai Kong⁵, Ryan Baumbach,⁴ Gabriel Kotliar,² Weiwei Xie^{1*}

¹Department of Chemistry and Chemical Biology, Rutgers University, Piscataway, NJ, 08854, USA

²Department of Physics and Astronomy, Rutgers University, Piscataway, NJ, 08854, USA

³Department of Physics, Chungnam National University, Daejeon, 34134, South Korea

⁴National High Magnetic Field Laboratory, Tallahassee, FL, 32310, USA

⁵Department of Physics, University of Arizona, Tucson, AZ 85721, USA

Abstract

We report the magnetic changes from canted antiferromagnetic to ferromagnetic orderings in anti-115-type $\text{MnPt}_{5-x}\text{Pd}_x\text{P}$ ($x = 1, 2, 2.5, 3, 4,$ and 5) and the discovery of a new rare-earth-free ferromagnet, MnPd_5P by both theoretical prediction and experimental investigation. The family compounds were synthesized using high temperature solid state method and characterized to crystallize in the anti-CeCoIn₅ type with the space group $P4/mmm$ exhibiting a two-dimensional layered structural feature. The magnetic property measurements indicate that the compounds ordered from canted A-type antiferromagnet in MnPt_5P to ferromagnet above the room temperature with varying degrees of coercivity and magnetic moments in MnPd_5P by reducing the spin orbital coupling. The results of the $\text{MnPt}_{5-x}\text{Pd}_x\text{P}$ have been analyzed in comparison to the other candidates of the 151 family of $\text{Mn}(\text{Pt}/\text{Pd})_5(\text{P}/\text{As})$ to understand the complex structure-magnetism relationships.

Keywords: 2D materials, chemical substitution, ferromagnetic, magnetic properties

Introduction

Ferromagnetic (FM) and antiferromagnetic (AFM) spintronics as well as the emerging fields of magnetic topological materials in atomically thin two-dimensional (2D) layers have attracted a great deal of experimental and theoretical interests among materials scientists, especially the magnetic anisotropy in 2D magnetism.[1,2] Such materials form a basis for most of the critical key quantum technology of future information. Most of materials are magnetic semiconductors or insulators, in which super-exchange interaction theories are widely used to explain the magnetism.[3] Very few low-dimensional itinerant magnetic metals which shows completely different electronic and magnetic properties from magnetic semiconductors have been reported and studied.[4–8] From a theoretical perspective, it is rather challenging to understand and, therefore, predict whether a structure containing transition metals will be Pauli paramagnetic, ferromagnetic, antiferromagnetic or even ferromagnetic.[9] Based on our previous experimental study, magnetically active *3d* metals occupying voids in complex intermetallic frameworks give rise to low-dimensional structures of these magnetic metals, which may result in low-dimensional magnetic behaviors, such as layered ferromagnetic MnPt₅As and antiferromagnetic MnPt₅P.[10,11]

The iso-valent MnPt₅As and MnPt₅P in the same crystal structure show completely different magnetic orderings. Both MnPt₅As and MnPt₅P crystalize in the CeCoIn₅-type tetragonal structure with the space group *P4/mmm*. [10,11] Different from CeCoIn₅, magnetic *3d* transition metals occupy Ce site while late transition metal Pt locates on the In site. Similar to heavy-fermion CeCoIn₅ system, MnPt₅As and MnPt₅P also show the large magnetic anisotropy along different directions.[10,11] The slight atomic radii differences between P and As completely changed the magnetic orderings in ferromagnetic MnPt₅As and antiferromagnetic MnPt₅P. This motivated us to investigate the lattice parameters effects on magnetic orderings by theoretical simulation and predict the magnetic interactions in the low-dimensional itinerant magnets.

To accelerate our search for various new magnetic materials, we employed the magnetic ordering and total energy calculation first to determine the thermodynamic stable magnetic ordering. Using the predicted atomic radii, we successfully synthesized the family compounds anti-115-type MnPt_{5-x}Pd_xP ($x = 1, 2, 2.5, 3, 4, \text{ and } 5$). Thus, the new ferromagnetic MnPd₅P with the Curie-Weiss temperature as high as ~305 K was found. The experimental structural and magnetic characterizations on MnPd₅P are consistent with the theoretical predictions.

Experimental Section

Synthesis: High temperature solid-state pellet method was utilized to synthesize the $\text{MnPt}_{5-x}\text{Pd}_x\text{P}$ ($x = 1, 2, 2.5, 3, 4,$ and 5). Mn powder (Mangan, 99+%), Pt powder (BTC, -22 mesh, 99.99%), Pd powder (BTC, -200 mesh, 99.95%) and red P powder (BTC, -100 mesh, 99%) were mixed and ground in Mn: Pt/Pd: P = 1:5:1 atomic ratio. The mixture was pressed into a $d=1/4$ pellet. The pellet was placed into an alumina crucible and sealed in an evacuated silica tube ($<10^{-5}$ Torr). The evacuated sample tube was then heated to 1050°C at a rate of 40°C per hour. After annealing for 2 days at 1050°C , it was slowly cooled down to room temperature at the speed of 10°C per hour. The polycrystalline $\text{MnPt}_{5-x}\text{Pd}_x\text{P}$ obtained was stable in air and moisture. The polycrystalline $\text{MnPt}_{5-x}\text{Pd}_x\text{P}$ was used for the structural characterization and physical property measurements.

Phase Determination and Structural Analysis: The phase identification of all $\text{MnPt}_{5-x}\text{Pd}_x\text{P}$ ($x = 1, 2, 2.5, 3, 4,$ and 5) polycrystalline samples were done by the Bruker D2 Phaser XE-T edition benchtop X-ray Powder Diffractometer equipped with Cu K_α , $\lambda=1.5405 \text{ \AA}$. Data was collected over a range of Bragg angle, 2θ , from 5 to 90° at a rate of $0.008^\circ/\text{s}$. LeBail fitting of Powder X-Ray Diffraction (PXRD) data was completed with the Fullprof Suite software for the initial phase identification and the lattice parameters determination.[12–14] Single crystal X-ray diffraction (SCXRD) experiments were conducted in D8 Quest Eco diffractometer with Mo radiation ($\lambda_{K\alpha} = 0.71073 \text{ \AA}$) equipped with Photon II detector. Single crystals were mounted on a Kapton loop and measured with an exposure time of 10 s per frame scanning 2θ width of 0.5° . Structure refinement was performed in SHELXTL package using direct method and full matrix least-squares on F^2 model.[15,16] Anisotropic thermal parameter for all atoms were refined in SHELXTL. The VESTA software was used to plot the crystal structures.[17]

Scanning Electron Microscope (SEM): Chemical compositions of $\text{MnPt}_{5-x}\text{Pd}_x\text{P}$ ($x = 1, 2, 2.5, 3, 4,$ and 5) samples were analyzed using a high vacuum Zeiss Sigma Field Emission SEM (FESEM) with Oxford INCA PentaFETx3 Energy-Dispersive Spectroscopy (EDS) system. Spectrums were collected for 100 s from multiple areas of the crystals mounted on a carbon tape with an accelerating voltage of 20 keV .

Physical Property Measurements: Magnetic properties of the polycrystalline $\text{MnPt}_{5-x}\text{Pd}_x\text{P}$ ($x = 1, 2, 2.5, 3, 4,$ and 5) was measured in Quantum Design PPMS Dynacool (QD-PPMS) at

National High Magnetic Field Laboratory over a temperature range of 1.8 to 400 K with the applied field of 1000 Oe. Additionally, magnetic measurements of Pt doped compounds were carried out in vibrating sample magnetometer (VSM) in Quantum Design PPMS system over a temperature range of 1.8 – 600 K with the applied field of 1000 Oe. Magnetic susceptibility is defined as $\chi = M/H$ where M is the magnetization in units of emu and H is the applied field. The field dependent magnetization measurements were carried out at different temperatures of 2 K, 100 K, 200 K, 300 K, 325 K and 350 K up to 90 kOe.

Theoretical Calculations: The all-electron full-potential linearized augmented plane-wave (FLAPW) method implemented in WIEN2k[18] was adopted to calculate the electronic structure. Experimental crystal structure was selected for calculations. Generalized gradient approximation (GGA) of Perdew-Burke-Ernzerhof (PBE)[19] was chosen for the exchange-correlation functional. A $20 \times 20 \times 11$ k -mesh was used for the Brillouin zone integration. The spin-orbit coupling (SOC) was included in the second-variational scheme. To consider the strong correlation effect in Mn 3d orbital, GGA+U was adopted within fully localized limit [20,21] The effective on-site Coulomb interaction parameter $U_{\text{eff}} = U - J = 5$ eV was used, where the Coulomb parameter was turned out to be valid in previous DFT calculations on another correlated Mn compounds.[22]

Results and Discussion

Total Energy Analysis of Magnetic Ground States of MnPt₅P and MnPt₅As: In the search of new magnetic materials in the anti-115 family, total energy analysis was adopted to determine the stable magnetic ordering. Moreover, to further understand structure-magnetism relationships and the nature of ground state properties of the new family in anti-CeCoIn₅ structure type, we analyzed total energy differences between the A-type antiferromagnetic (AFM1) ordering and ferromagnetic (FM) orderings ($\Delta E_{\text{AFM1-FM}}$) in MnPt₅As and MnPt₅P. The $\Delta E_{\text{AFM1-FM}}$ was calculated as a function of the lattice parameter c/a ratio with keeping the lattice parameter a constant for each compound. It should be noted that according to the experimental results in the family, the effect on lattice parameter a is negligible when X is changed in the MnT₅X (X = P, As) system due to the 2D layered nature of these materials while the effect on c axis is non-negligible. The total energy differences computed from the first-principle calculations with spin-orbit coupling (SOC) and the effective on-site Coulomb parameter U of $U = 0$ eV and $U = 5$ eV on MnPt₅P and MnPt₅As are shown in **Figure 1**.

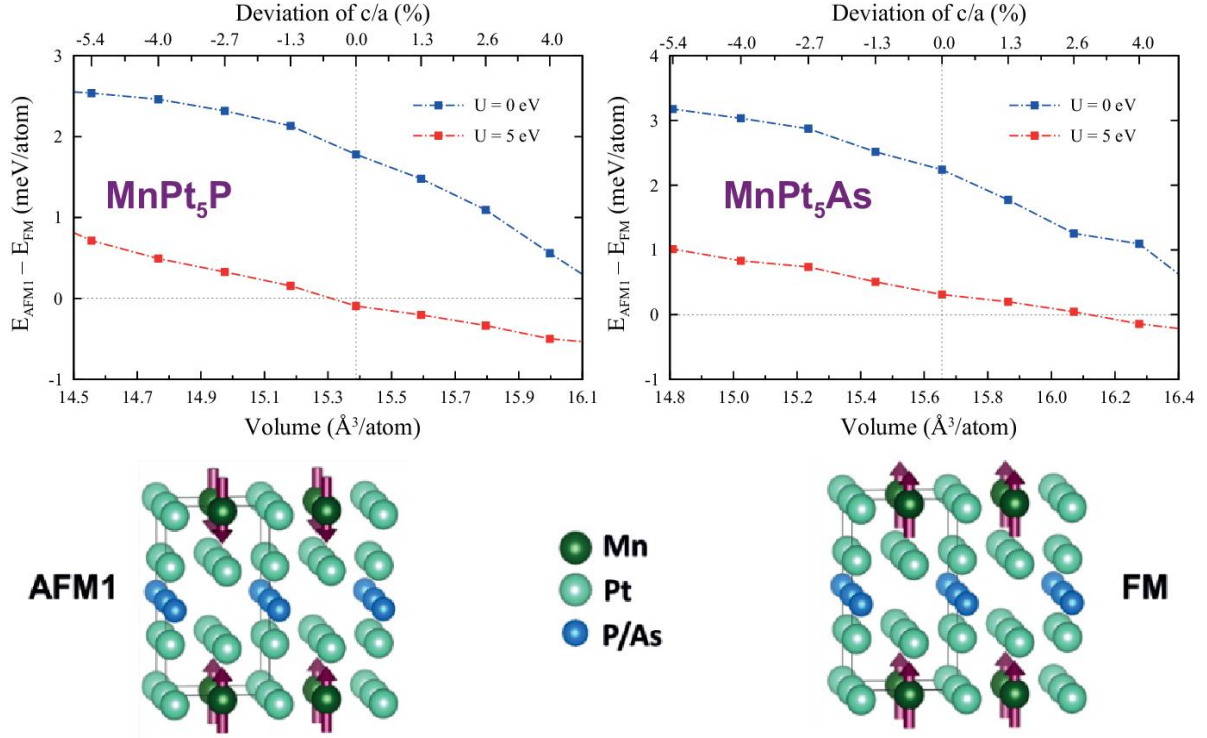


Figure 1. Results from GGA+SOC+U calculation by changing c/a ratio with a fixed lattice constant a for (a) MnPt_5P and (b) MnPt_5As with the illustration of spin orientation in ferromagnetic (FM) and the A-type antiferromagnetic (AFM1) ordering.

The computational results show the magnetic ground state for both compounds. The electronic correlation affects their magnetic ground state as demonstrated in the $U = 5$ eV calculations (see Figure 1). In the case of MnPt_5As , FM ordering is preferred regardless of the strength of the correlation at $\Delta c/a = 0.0$, while the a-type AFM ordering is favorable in the presence of the correlation ($U = 5$ eV) above $\Delta c/a \sim 2.6\%$. On the other hand, MnPt_5P shows the a-type AFM (AFM1) ordering at $\Delta c/a = 0.0$ in the presence of the correlation ($U = 5$ eV), but it is close to a border of the AFM1 and FM phases. Interestingly, a new ground-state with FM ordering emerges at $\Delta c/a \sim -0.5\%$. With these theoretical predictions in mind, we aim to replace Pt with slightly smaller Pd in anti-115 system to explore new itinerant ferromagnetic material in our experiments. Initial structural and magnetic property measurements on $\text{MnPt}_{5-x}\text{Pd}_x\text{P}$ ($x = 1, 2, 2.5, 3, 4, \text{ and } 5$) confirm the magnetic changes from antiferromagnetism to ferromagnetism. Furthermore, the new anti-115 MnPd_5P hosts the FM state at room temperature

Single Crystal Structure Determination and Phase Analysis: The variants of anti-115 $\text{MnPt}_{5-x}\text{Pd}_x\text{P}$ ($x = 1, 2, 2.5, 3, 4, \text{ and } 5$) samples were successfully synthesized using solid-state pellet reaction and structurally characterized utilizing SCXRD measurements. The resulting

crystallographic data including atomic coordinates, site occupancies and equivalent isotropic thermal displacement parameters of MnPd₅P is reported in the **Table 1 and 2** while crystallographic information on MnPt_{5-x}Pd_xP ($x = 1, 2, 2.5, 3, \text{ and } 4$) compounds are given in the **Table S1 and S2**. The results indicate that MnPt_{5-x}Pd_xP ($x = 1, 2, 2.5, 3, 4, \text{ and } 5$) crystallize in a tetragonal unit cell with the space group of $P4/mmm$ the same as the previously reported MnPt₅P and MnPt₅As compounds in anti-CeCoIn₅-type structure. The refined lattice parameters for MnPd₅P are $a=3.899$ (2) Å and $c=6.867$ (4). As shown in the **Figure 2a**, MnPd₅P adopts a layered structure with alternating layers of Mn@Pd₁₂ face sharing polyhedral and P layers.

Table 1. Single crystal structure refinement for MnPd₅P at 300(2) K. (Standard deviation is indicated by the values in parentheses)

Refined Formula	MnPd ₅ P
F.W. (g/mol)	617.91
Space group; Z	$P 4/mmm$; 1
a (Å)	3.899 (2)
c (Å)	6.867 (4)
V (Å ³)	104.42 (9)
θ range (°)	2.966-34.770
No. reflections; R_{int}	578; 0.0609
No. independent reflections	170
No. parameters	12
R_1 ; ωR_2 ($I > 2\delta(I)$)	0.0509; 0.1204
Goodness of fit	1.282
Diffraction peak and hole (e ⁻ /Å ³)	2.656; -1.863

Table 2. Atomic coordinates and equivalent isotropic displacement parameters of MnPd₅P at 300(2) K. (U_{eq} is defined as one-third of the trace of the orthogonalized U_{ij} tensor (Å²)).

Atom	Wyckoff.	Occ.	x	y	z	U_{eq}
Pd1	$4i$	1	0	$\frac{1}{2}$	0.2948 (1)	0.015(1)
Pd2	$1a$	1	0	0	0	0.012(2)
Mn3	$1c$	1	$\frac{1}{2}$	$\frac{1}{2}$	0	0.022(1)
P4	$1b$	1	0	0	$\frac{1}{2}$	0.016(2)

Table 3. The comparison of structural – property features of MnPd₅P with MnPt₅P and MnPt₅As.

	MnPd ₅ P	MnPt ₅ P	MnPt ₅ As
<i>c/a</i> ratio	1.761	1.779	1.816
Shortest Mn-Mn distance (<i>ab</i> plane)/ Å	3.899 (2)	3.896 (2)	3.903 (2)
Interlayer Mn-Mn distance/ Å	6.867 (4)	6.931 (2)	7.091 (3)
Volume / Å³	104.42 (9)	105.25 (1)	109.58 (5)
Mn-Pt/Pd distance in Mn@(Pd/Pt)₁₂/Å			
<i>ab</i> plane	2.757 (3)	2.755 (1)	2.779 (2)
Out of <i>ab</i> plane	2.810 (2)	2.807 (1)	2.790 (1)
P-Pd/Pt/ Å	2.405 (2)	2.425 (1)	2.512 (1)
Magnetic ordering	FM	AFM	FM
Transition temperature/ K	299 (2)	188 (2)	300 (2)

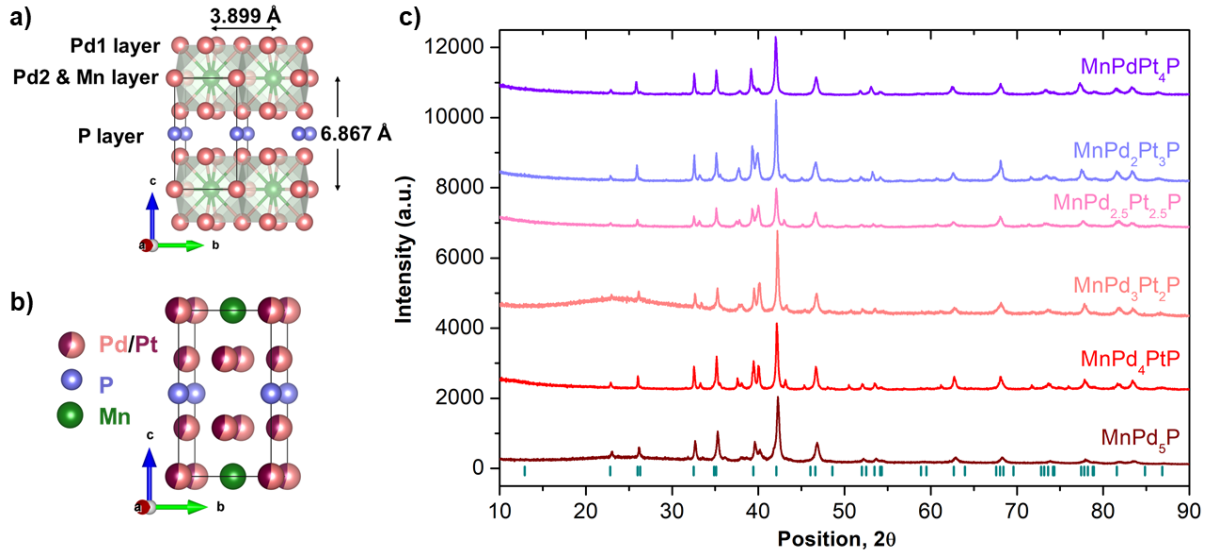


Figure 2. (a) The crystal structure of MnPd₅P showing Mn@Pd₁₂ face sharing polyhedral and P layers (b) Unit cell of MnPt_{5-x}Pd_xP indicating the mixture of Pd and Pt. (c) Powder diffraction patterns of MnPt_{5-x}Pd_xP ($x = 1, 2, 2.5, 3, 4,$ and 5). The green vertical bars mark the expected Bragg positions for MnPd₅P.

Pd substitutions on MnPt₅P yielded five new compounds with nominal compositions of MnPt_{5-x}Pd_xP ($x = 1, 2, 2.5, 3, 4$). These compounds were structurally characterized to maintain the parent lattice structure with different distribution of Pt/Pd mixture on the two atomic sites 1a and 1b as indicated in **Figure 2b**. Details on the Pt/Pd distributions on 1a and 1b sites for each phase are given in the **Table S2**. The single crystal refinement results on Pd doped samples indicated some residual intensities on the 1a and 1b sites even after mixed occupancy of Pt/Pd

is accounted. This observation suggests a possibility of Pd-Pt solid solution like nature on these materials rather than a completely ordered structure. This also provides an explanation for the refined high diffraction peak and hole values and goodness of fit for some of the $\text{MnPt}_{5-x}\text{Pd}_x\text{P}$ single crystal data which could originate from mismatch between the model and the actual structure. Moreover, synthesizing high quality single crystals for these compounds were a challenge and for MnPdPt_4P irrespective of multiple synthesis attempts, we were unable to grow high quality single crystals to collect data to refine the structure, as a result only the lattice parameters are reported in **Table S1**. However, the SCXRD results, and chemical compositions can be further supported by the PXRD and SEM-EDX analysis. A comparison of PXRD for $\text{MnPt}_{5-x}\text{Pd}_x\text{P}$ ($x = 1, 2, 2.5, 3, 4,$ and 5) phases with the calculated Bragg peaks for the parent MnPd_5P phase are presented in **Figure 2c**. The LeBail fitting of PXRD for MnPd_5P is given in the **Figure S1**. The refined lattice parameters for MnPd_5P are in well agreement with the single crystal refinement data ($\chi^2 = 1.99$). PXRD analysis shows the high purity of the bulk MnPd_5P phase. The possible impurity phases of Pd and MnPd_3 were tested in the refinement and confirmed the synthesis of pure phase MnPd_5P . The percentage of impurities in $\text{MnPt}_{5-x}\text{Pd}_x\text{P}$ samples were evaluated from the Rietveld refinement in the HighScore Plus software. Results indicate that loaded MnPd_4PtP , $\text{MnPd}_3\text{Pt}_2\text{P}$, $\text{MnPd}_{2.5}\text{Pt}_{2.5}\text{P}$, $\text{MnPd}_2\text{Pt}_3\text{P}$ and MnPdPt_4P reactions yielded 86.8%, 82.7%, 51.2%, 75.8% and 93.1% of the targeted phase as the major phase respectively. The Cubic PdPt impurity was observed in all $\text{MnPt}_{5-x}\text{Pd}_x\text{P}$ ranging from 2-20% which further supports our speculation from SCXRD results about the Pd-Pt solid solution nature in these materials. However, the magnetic impurities MnPdP and MnPt were found to consist less than 5% in all doped samples except for $\text{MnPd}_{2.5}\text{Pt}_{2.5}\text{P}$ which was 32%. Detailed Rietveld refinement analysis with impurities is given in **Table S2**.

The chemical compositions and the stoichiometries were further evaluated using SEM-EDS and details are reported in **Table S3**. The chemical composition determined by SEM-EDS gives $\text{Mn}_{1.00}\text{Pd}_{4.73}\text{P}_{0.79}$, $\text{Mn}_{1.00}\text{Pd}_{3.99}\text{Pt}_{0.96}\text{P}_{0.88}$, $\text{Mn}_{1.00}\text{Pd}_{2.88}\text{Pt}_{2.01}\text{P}_{0.84}$, $\text{Mn}_{1.00}\text{Pd}_{2.48}\text{Pt}_{2.46}\text{P}_{0.83}$, $\text{Mn}_{1.00}\text{Pd}_{1.82}\text{Pt}_{2.82}\text{P}_{0.78}$, and $\text{Mn}_{1.00}\text{Pd}_{0.92}\text{Pt}_{3.96}\text{P}_{0.82}$ for the loaded Pt mol% of 0%, 14.2%, 28.5%, 35.7%, 42.8% and 57.1% respectively. Furthermore, these results are in good agreement with the single crystal results given in **Table 1 and Table S1**.

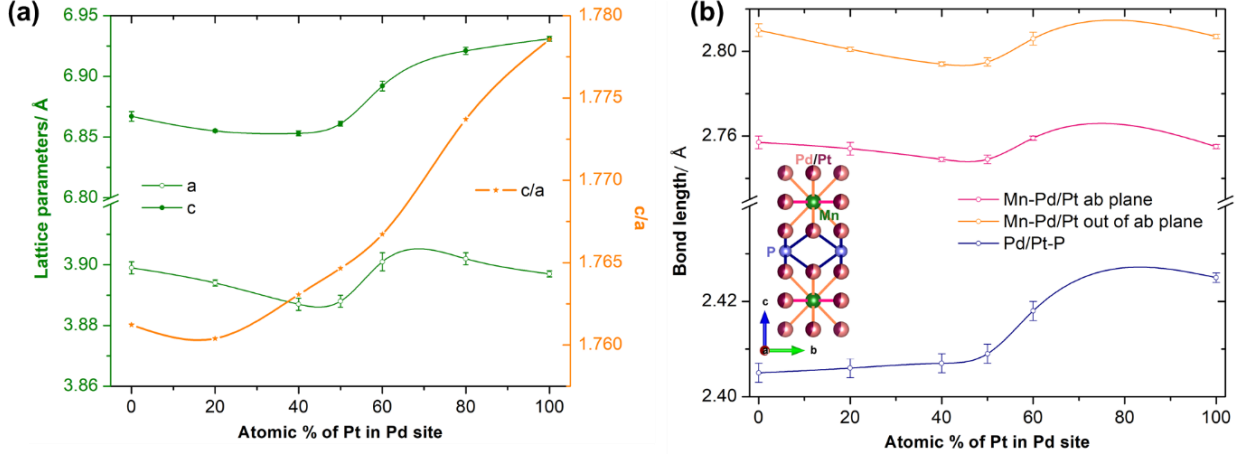


Figure 3. The comparison of structural features of $\text{MnPt}_{5-x}\text{Pd}_x\text{P}$ ($x = 1, 2, 3, 4$ and 5) with MnPt_5P showing (a) change of lattice parameters and c/a ratios (b) change of atomic bond distances within $\text{Mn}@\text{(Pt/Pd)}_{12}$ with changing Pd content.

A comparison of the structural features of the new anti-115-Pd variants with the related MnPt_5P structure are given in **Figure 3**. As shown in **Figure 3a**, the lattice parameter a is almost constant (3.899 ± 0.004) in all compounds consequently leading to similar Mn-Mn distance in the ab plane while the c parameter of the new compounds $\text{MnPt}_{5-x}\text{Pd}_x\text{P}$ has shortened $\sim 1\%$ compared to MnPt_5P . Moving from $5d$ (Pt) to $4d$ (Pd) has not significantly changed the ab -plane of the structure due to the close atomic size of Pt to Pd caused by the lanthanide contraction and shielding of Pt. Overall, the $\text{Mn}@\text{(Pd/Pt)}_{12}$ shows similar features in all compounds as indicated in **Figure 3b**. Interestingly, the c axis is sensitive to the changes in chemical composition leading to different magnetic properties in each compound, ranging from canted antiferromagnetic MnPt_5P to ferromagnetic MnPd_5P in this family.

Vanishing Spin-Canting by Replacing Pt with Pd: The spin-canted antiferromagnetic ordering was detected in MnPt_5P with the $T_N \sim 188$ K by our previous work.[10] However, at 350 K, the ferromagnetic component along the c -axis still exists in MnPt_5P . By replacing Pt with Pd up to 40%, the ferromagnetic transition appears at ~ 354 K (20% Pd) and ~ 366 K (40% Pd), while the spin-canting temperature increases to ~ 246 K (20% Pd) and ~ 299 K (40% Pd) respectively. Once the Pd replaces 50% of Pt, the spin-canting disappears, and only the ferromagnetic transition was observed around 300 K. The polycrystalline samples of $\text{MnPt}_{5-x}\text{Pd}_x\text{P}$ were used to measure the magnetic properties with an external magnetic field of 1000 Oe from 1.8 K to 350 K/ 400 K or 600 K as required. The zero-field cooling (ZFC) and field

cooling (FC) graphs of the magnetic susceptibility (χ) vs temperature collected below 350 K are shown in the **Figure 4** q χ vs T for all compounds are given in **Figure S2**. Upon cooling each sample, a dramatic increase in magnetic susceptibility was observed around room temperature or above suggesting the ferromagnetic ordering of all $\text{MnPt}_{5-x}\text{Pd}_x\text{P}$ compounds. The transition temperature (T_c) for each composition is plotted against the atomic % of Pt in each material and given in the **Figure 5** which are ranging from ~ 299 to ~ 366 K. The T_c of each compound was determined using the derivative of χ vs T. As indicated in the **Figure 5**, the T_c of these materials increase with increasing Pt content, reach the maximum around 30% before it starts decreasing around 40%. Starting from 300 K in MnPd_5P , T_c of MnPd_4PtP increased to about 316 K before it starts lowering from $\text{MnPd}_3\text{Pt}_2\text{P}$ and onwards. Furthermore, when the Pt content is above 50 %, two transitions were observed for $\text{MnPd}_2\text{Pt}_3\text{P}$ and MnPdPt_4P compounds. T_{c1} and T_{c2} for $\text{MnPd}_2\text{Pt}_3\text{P}$ are found to be 366 K and 299 K while for MnPdPt_4P , it was 354 K and 246 K respectively. Furthermore, in MnPt_5P , AFM transition $T_N \sim 188$ K is reported while results evident that FM interactions along c axis are still there above 350 K as χ has not reached zero.[10] Therefore, for the FM transition in MnPt_5P , a hypothetical value above 350 K has used to depict how the two transitions from canted AFM merge in to the purely FM transition in MnPd_5P with increasing Pd content in **Figure 5**. This indicates that by lowering the Pt content, the gap between T_{c1} and T_{c2}/T_N has lowered upto 40 % Pt, merging to one transition around 50 % Pt disappearing the AFM interactions in the $\text{MnPt}_{5-x}\text{Pd}_x\text{P}$ system. Moreover, when the materials with single T_c , $\text{MnPt}_{5-x}\text{Pd}_x\text{P}$ ($x = 2.5, 3, 4, 5$) are considered, it is revealed that the system has the highest T_c when c/a ratio is minimum while the highest c/a ratio yielded an antiferromagnet MnPt_5P . Similar magnetic crossovers from AFM to FM has been observed in Mn sublattice in YbMn_6Sn_6 system with HfFe_6Ge_6 type structure where tuning the valance electron concentrations through chemical substitution of Yb site drives this magnetic behavior.[23–25] In $\text{SrCo}_2(\text{Ge}_{1-x}\text{P}_x)_2$ system where both SrCo_2P_2 and SrCo_2Ge_2 are paramagnetic, weak itinerant ferromagnetism has developed by the use of chemical bond breaking as a tuning parameter.[26–28] Additionally, introduction of Eu into AFM PrCo_2P_2 has pushed the material into an itinerant FM $\text{Pr}_{0.8}\text{Eu}_{0.2}\text{Co}_2\text{P}_2$ due to a strong chemical compression.[29,30] It is clear that magnetic crossovers in the systems can be manipulated through various parameters while the observed AFM to FM transformation in $\text{MnPt}_{5-x}\text{Pd}_x\text{P}$ system is driven by tuning the unit cell dimensions and spin-orbit coupling effects.

A significant difference in the ZFC and FC measurements at 1000 Oe was not observed in MnPd₅P while all Pt doped compounds indicated a split of ZFC, and FC measurements as shown in **Figure 4a-f**. Previous studies have shown that in some ferromagnetic systems such as perovskites SrRuO₃, La_{0.7}Ca_{0.3}MnO₃ and La_{0.5}Sr_{0.5}CoO₃, the irreversibility indicated by the difference in ZFC and FC magnetic susceptibilities result from magnetic anisotropy.[31] Accordingly, when using this as a measure of magnetic anisotropy, it is clear that MnPd₅P shows minimum magnetic anisotropy while all Pt doped variants possesses magnetic anisotropy to varying extents in the system as a result of higher spin-orbit coupling contribution from Pt.

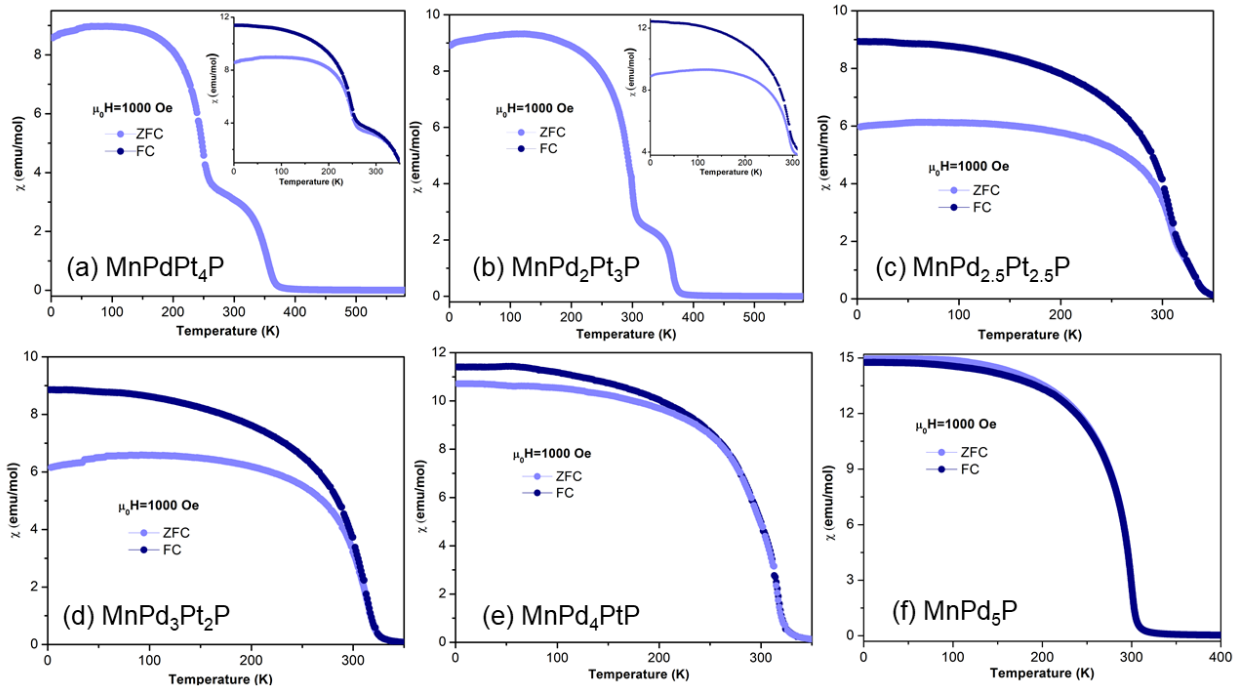


Figure 4. Magnetic susceptibility versus temperature measured by zero field cooled (ZFC) and field cooled (FC) methods at 1000 Oe for (a) MnPdPt₄P (b) MnPd₂Pt₃P (c) MnPd_{2.5}Pt_{2.5}P (d) MnPd₃Pt₂P (e) MnPd₄PtP and (f) MnPd₅P. For (a) and (b) the main panel shows the combined ZFC χ measurements at low temperatures and high temperatures while the insets represent ZFC and FC graphs measured below room temperature.

The high temperature region of the magnetic susceptibility data was analyzed by and the Curie-Weiss law, $\chi = \frac{C}{T - \theta_{CW}}$ and the fitting for each material is given in **Figure S3**. The symbols, χ , C , and θ_{CW} represent magnetic susceptibility, temperature independent contribution to the susceptibility, Curie constant and the Curie-Weiss temperature, respectively. The effective magnetic moments (μ_{eff} per Mn atom) ($\mu_{eff} = \sqrt{8C} \mu_B$) calculated from Curie-Weiss fitting is

given in in the **Table 4**. MnPd₅P indicate a higher $\mu_{eff} \sim 5\mu_B$ than $\sim 3.5\mu_B$ observed in ferromagnetically ordered MnPt₅As from the same family.[11] The fitted Curie-Weiss temperatures are in a close agreement with the observed ferromagnetic transitions for each composition.

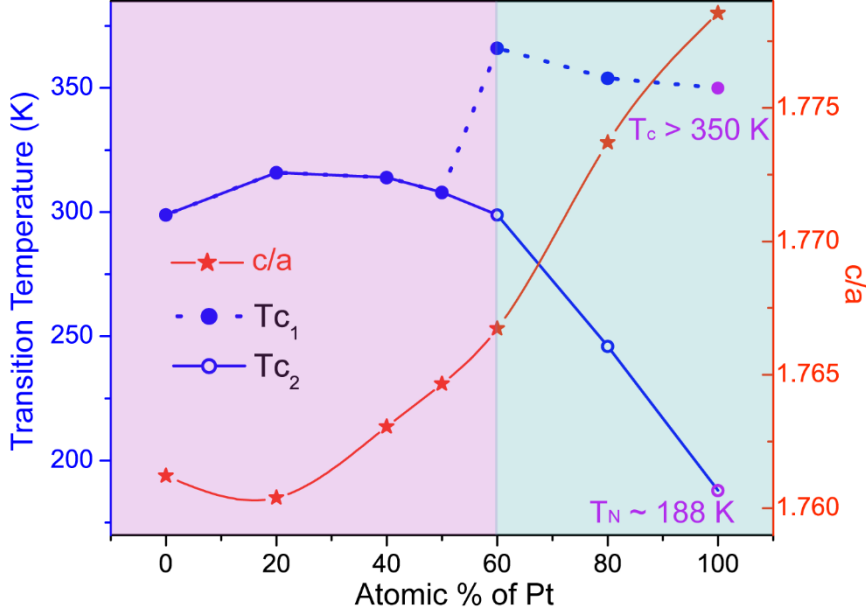


Figure 5. The trend of transition temperatures of MnPd₅P, MnPt_{5-x}Pd_xP and MnPt₅P relative to the change of c/a ratio.

The field dependent magnetization measurement of the MnPt_{5-x}Pd_xP ($x = 1, 2, 2.5, 3, 4, 5$) is shown in **Figure 6**. The hysteresis loops of magnetization were measured at different temperatures ranging from 2 K to 350 K with the external fields up to 90 kOe. The isothermal magnetization curves at 2 K tend to saturate around $\sim 4\mu_B$ /Mn by the applied external field of ~ 1 T for all compounds. With the increasing temperature saturated magnetic moments gradually decreases upto room temperature (300 K) and disappears above 325 K for MnPt_{5-x}Pd_xP ($x = 1, 2, 2.5, 3, 4, 5$). However, for compounds MnPd₂Pt₃P and MnPdPt₄P magnetic moments tend to saturate upto 350 K. These results further support that all MnPt_{5-x}Pd_xP ($x = 1, 2, 2.5, 3, 4, 5$) compounds are ferromagnets above room temperature. The coercivity of each compound at 2 K is presented in **Figure 7a**. The results indicate that all MnPt_{5-x}Pd_xP ($x = 1, 2, 2.5, 3, 4, 5$) compounds can be categorized into semi-hard ferromagnets as their coercivities are in the range 13 Oe – 376 Oe.[5] This is unlike the soft ferromagnetism observed in MnPt₅As.[11] The change of coercivities with respect to Pt content in the structure is represented in the **Inset** of **Figure 7** suggesting a non-linear dependence. The critical fields and

maximum magnetization derived from isothermal magnetization curves at 2 K are shown in **Figure 7b** which indicates a non-linear dependence in $\text{MnPt}_{5-x}\text{Pd}_x\text{P}$ system unlike for the Mn sublattice in YbMn_6Sn_6 system.[23,25]

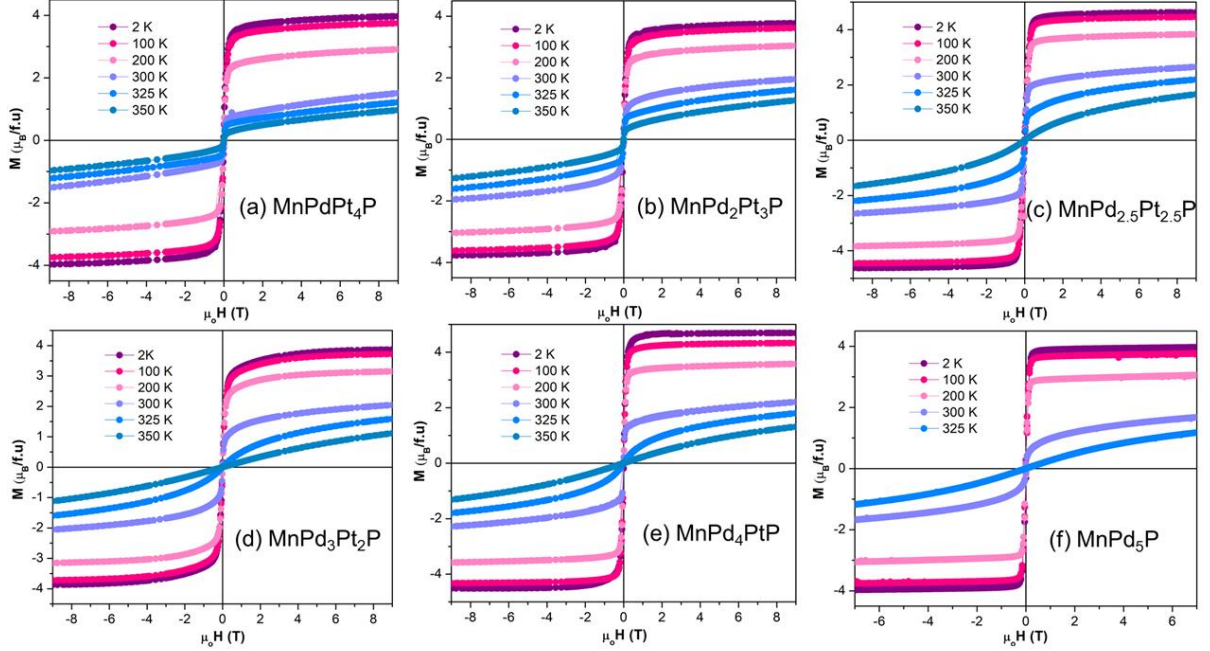


Figure 6. Magnetization vs applied field at temperatures of 2, 100, 200, 300, 325 and 350 K for (a) MnPt_4PdP (b) $\text{MnPt}_3\text{Pt}_2\text{P}$ (c) $\text{MnPt}_{2.5}\text{Pd}_{2.5}\text{P}$ (d) $\text{MnPt}_2\text{Pd}_3\text{P}$ (e) MnPtPd_4P and (f) MnPd_5P

Table 4. Summary of magnetic parameters derived from Curie-Weiss fitting

	MnPd_5P	MnPd_4PtP	$\text{MnPd}_3\text{Pt}_2\text{P}$	$\text{MnPd}_{2.5}\text{Pt}_{2.5}\text{P}$	$\text{MnPd}_2\text{Pt}_3\text{P}$	MnPdPt_4P	MnPt_5P
T_N (K)	/	/	/	/	299	246	188
T_c (K)	300	316	314	308	366	354	>350
θ_{CW} (K)	304.4(1)	317.8(3)	318.0(1)	334.1(2)	369.9(1)	366.2(3)	
C	3.13(1)	4.14(6)	2.45(1)	2.09(4)	1.09(1)	1.16(1)	
μ_{eff} (μ_B)	5.00	5.75	4.43	4.09	2.95	3.04	
Coercivity (Oe)	~93	~68	~91	~77	~52	~68	

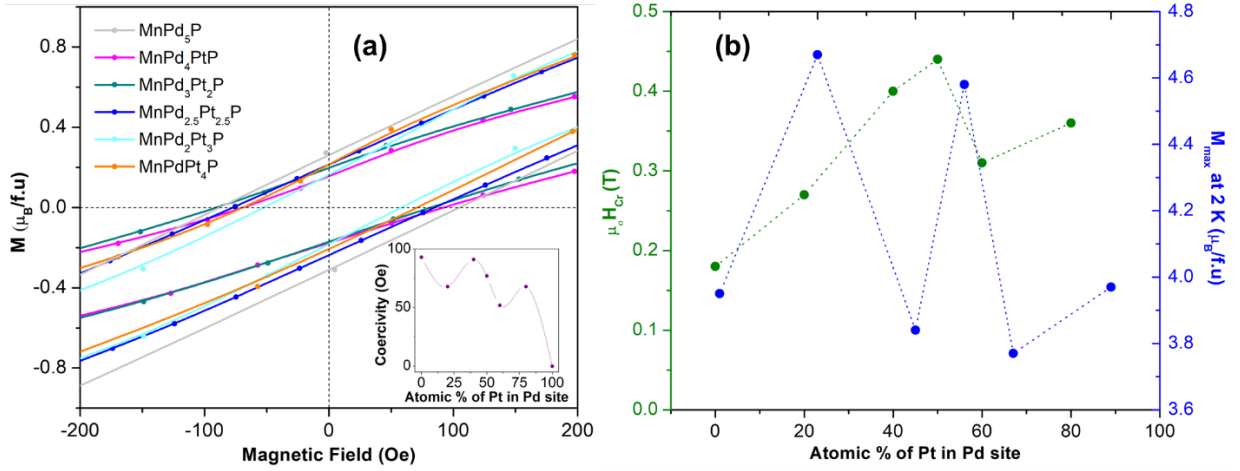


Figure 7. (a) Hysteresis loops measured under low field at 2 K for each compound MnPt_{5-x}Pd_xP ($x = 1, 2, 2.5, 3, 4, 5$). *Inset* showing the change of coercivity of with the Pt content in the anti-115 compounds. (b) Critical field ($\mu_0 H_{Cr}$) on the left axis and maximum magnetization on the right axis extracted from isothermal magnetization at 2 K for MnPt_{5-x}Pd_xP ($x = 1, 2, 2.5, 3, 4, 5$). The lines are only eye guides.

Conclusion

We have successfully synthesized the family compounds MnPt_{5-x}Pd_xP ($x = 1, 2, 2.5, 3, 4, 5$) using high temperature solid state synthesis method, characterized the structural and magnetic properties of the materials. MnPd₅P in the anti-CeCoIn₅-system was theoretically predicted and experimentally confirmed to show stable ferromagnetic properties. MnPd₅P is a low dimensional itinerant ferromagnet with a Curie-Weiss temperature of ~ 305 K and semi-hard magnetic nature. This study provides a new platform in addition to the widely studied CeCoIn₅-structure type to understand the tunability of structure and magnetism and predict new rare-earth free magnets.

Acknowledgements

The work at Rutgers is supported by Beckman Young Investigator award and NSF-DMR-2053287. C. -J.K. and G.K. were supported by the U.S. Department of Energy, Office of Science (Basic Energy Science) as a part of the Computational Materials Science Program through the Center for Computational Design of Functional Strongly Correlated Materials and Theoretical Spectroscopy under DOE grant no. DE-FOA-0001276. C.-J.K. also acknowledges support by NRF grant No. 2022R1C1C1008200. A portion of this work was performed at the

National High Magnetic Field Laboratory, which is supported by National Science Foundation Cooperative Agreement No. DMR-1644779 and the State of Florida.

Conflicts of interest

The authors declare that there is no conflict of interest.

References

- [1] T. Jungwirth, X. Marti, P. Wadley, J. Wunderlich, Antiferromagnetic spintronics, *Nat. Nanotechnol.* 11 (2016) 231–241. <https://doi.org/10.1038/nnano.2016.18>.
- [2] T. Dietl, Functional ferromagnets, *Nat. Mater.* 2 (2003) 646–648. <https://doi.org/10.1038/nmat989>.
- [3] T. Dietl, A ten-year perspective on dilute magnetic semiconductors and oxides, *Nat. Mater.* 9 (2010) 965–974. <https://doi.org/10.1038/nmat2898>.
- [4] Z. Fei, B. Huang, P. Malinowski, W. Wang, T. Song, J. Sanchez, W. Yao, D. Xiao, X. Zhu, A.F. May, W. Wu, D.H. Cobden, J.-H. Chu, X. Xu, Two-dimensional itinerant ferromagnetism in atomically thin Fe_3GeTe_2 , *Nat. Mater.* 17 (2018) 778–782. <https://doi.org/10.1038/s41563-018-0149-7>.
- [5] Y. Zhang, G.J. Miller, B.P.T. Fokwa, Computational Design of Rare-Earth-Free Magnets with the $\text{Ti}_3\text{Co}_5\text{B}_2$ -Type Structure, *Chem. Mater.* 29 (2017) 2535–2541. <https://doi.org/10.1021/acs.chemmater.6b04114>.
- [6] P. Shankhari, J.P. Scheifers, M. Hermus, K. Yubuta, B.P.T. Fokwa, Unexpected Trend Deviation in Isoelectronic Transition Metal Borides $\text{A}_3\text{T}_5\text{B}_2$ (A = group 4, T = group 9): $\text{Ti}_3\text{Co}_5\text{B}_2$ - vs. Perovskite-Type Studied by Experiments and DFT Calculations, *Z. Für Anorg. Allg. Chem.* 643 (2017) 1551–1556. <https://doi.org/10.1002/zaac.201700271>.
- [7] B. Chen, J. Yang, H. Wang, M. Imai, H. Ohta, C. Michioka, K. Yoshimura, M. Fang, Magnetic Properties of Layered Itinerant Electron Ferromagnet Fe_3GeTe_2 , *J. Phys. Soc. Jpn.* 82 (2013) 124711. <https://doi.org/10.7566/JPSJ.82.124711>.
- [8] B.P.T. Fokwa, H. Lueken, R. Dronskowski, Rational Design of Complex Borides – One-Electron-Step Evolution from Soft to Semi-Hard Itinerant Ferromagnets in the New Boride Series $\text{Ti}_2\text{FeRu}_{5-n}\text{Rh}_n\text{B}_2$ ($1 \leq n \leq 5$), *Eur. J. Inorg. Chem.* 2011 (2011) 3926–3930. <https://doi.org/10.1002/ejic.201100315>.
- [9] G.D. Samolyuk, G.J. Miller, Relation between chemical bonding and exchange coupling approaches to the description of ordering in itinerant magnets, *J. Comput. Chem.* 29 (2008) 2177–2186. <https://doi.org/10.1002/jcc.21045>.
- [10] X. Gui, R.A. Klein, C.M. Brown, W. Xie, Chemical Bonding Governs Complex Magnetism in MnPt_5P , *Inorg. Chem.* 60 (2021) 87–96. <https://doi.org/10.1021/acs.inorgchem.0c02403>.
- [11] X. Gui, W. Xie, Crystal Structure, Magnetism, and Electronic Properties of a Rare-Earth-Free Ferromagnet: MnPt_5As , *Chem. Mater.* 32 (2020) 3922–3929. <https://doi.org/10.1021/acs.chemmater.0c00244>.
- [12] A. Le Bail, H. Duroy, J.L. Fourquet, Ab-initio structure determination of LiSbWO_6 by X-ray powder diffraction, *Mater. Res. Bull.* 23 (1988) 447–452.
- [13] R.E. Dinnebier, S.J.L. Billinge, Chapter 1. Principles of Powder Diffraction, in: R.E. Dinnebier, S.J.L. Billinge (Eds.), *Powder Diffraction*, Royal Society of Chemistry, Cambridge, 2008: pp. 1–19. <https://doi.org/10.1039/9781847558237-00001>.

- [14] R.E. Dinnebier, S.J.L. Billinge, *Powder Diffraction: Theory and Practice*, Royal Society of Chemistry, 2008.
- [15] G.M. Sheldrick, Crystal structure refinement with SHELXL, *Acta Crystallogr. Sect. C Struct. Chem.* 71 (2015) 3–8. <https://doi.org/10.1107/S2053229614024218>.
- [16] R. Herbst-Irmer, A. Spek, T. Schneider, M. Sawaya, *Crystal Structure Refinement: A Crystallographer's Guide to SHELXL*, OUP Oxford, 2006.
- [17] K. Momma, F. Izumi, VESTA: a three-dimensional visualization system for electronic and structural analysis, *J. Appl. Crystallogr.* 41 (2008) 653–658. <https://doi.org/10.1107/S0021889808012016>.
- [18] P. Blaha, K. Schwarz, F. Tran, R. Laskowski, G.K.H. Madsen, L.D. Marks, WIEN2k: An APW+lo program for calculating the properties of solids, *J. Chem. Phys.* 152 (2020) 074101. <https://doi.org/10.1063/1.5143061>.
- [19] J.P. Perdew, K. Burke, M. Ernzerhof, Generalized Gradient Approximation Made Simple, *Phys. Rev. Lett.* 77 (1996) 3865–3868. <https://doi.org/10.1103/PhysRevLett.77.3865>.
- [20] V.I. Anisimov, I.V. Solovyev, M.A. Korotin, M.T. Czyżyk, G.A. Sawatzky, Density-functional theory and NiO photoemission spectra, *Phys. Rev. B.* 48 (1993) 16929–16934. <https://doi.org/10.1103/PhysRevB.48.16929>.
- [21] V.I. Anisimov, F. Aryasetiawan, A.I. Lichtenstein, First-principles calculations of the electronic structure and spectra of strongly correlated systems: the LDA+U method, *J. Phys. Condens. Matter.* 9 (1997) 767–808. <https://doi.org/10.1088/0953-8984/9/4/002>.
- [22] A. Floris, S. de Gironcoli, E.K.U. Gross, M. Cococcioni, Vibrational properties of MnO and NiO from DFT +U -based density functional perturbation theory, *Phys. Rev. B.* 84 (2011) 161102. <https://doi.org/10.1103/PhysRevB.84.161102>.
- [23] L. Eichenberger, P. Haraux, G. Venturini, B. Malaman, T. Mazet, Structural and magnetic properties of the new Yb_{1-x}Sc_xMn₆Sn₆ solid solution, *J. Alloys Compd.* 775 (2019) 883–888. <https://doi.org/10.1016/j.jallcom.2018.10.208>.
- [24] G. Venturini, B.C.E. Idrissi, B. Malaman, Magnetic properties of RMn₆Sn₆ (R = Sc, Y, Gd–Tm, Lu) compounds with HfFe₆Ge₆ type structure, *J. Magn. Magn. Mater.* 94 (1991) 35–42. [https://doi.org/10.1016/0304-8853\(91\)90108-M](https://doi.org/10.1016/0304-8853(91)90108-M).
- [25] L. Eichenberger, G. Venturini, B. Malaman, L. Nataf, F. Baudelet, T. Mazet, Commensurate-incommensurate magnetic phase transition in the new Yb_{1-x}Lu_xMn₆Sn₆ compounds, *J. Alloys Compd.* 695 (2017) 286–293. <https://doi.org/10.1016/j.jallcom.2016.10.191>.
- [26] S. Jia, P. Jiramongkolchai, M.R. Suchomel, B.H. Toby, J.G. Checkelsky, N.P. Ong, R.J. Cava, Ferromagnetic quantum critical point induced by dimer-breaking in SrCo₂(Ge_{1-x}P_x)₂, *Nat. Phys.* 7 (2011) 207–210. <https://doi.org/10.1038/nphys1868>.
- [27] M. Imai, C. Michioka, H. Ohta, A. Matsuo, K. Kindo, H. Ueda, K. Yoshimura, Anomalous itinerant-electron metamagnetic transition in the layered Sr_(1-x)Ca_(x)Co₂P₂ system, *Phys. Rev. B.* 90 (2014) 014407. <https://doi.org/10.1103/PhysRevB.90.014407>.
- [28] S. Jia, A.J. Williams, P.W. Stephens, R.J. Cava, Lattice collapse and the magnetic phase diagram of Sr_(1-x)Ca_xCo₂P₂, *Phys. Rev. B.* 80 (2009) 165107. <https://doi.org/10.1103/PhysRevB.80.165107>.
- [29] K. Kovnir, W.M. Reiff, A.P. Menushenkov, A.A. Yaroslavtsev, R.V. Chernikov, M. Shatruk, “Chemical Metamagnetism”: From Antiferromagnetic PrCo₂P₂ to Ferromagnetic Pr_{0.8}Eu_{0.2}Co₂P₂ via Chemical Compression, *Chem. Mater.* 23 (2011) 3021–3024. <https://doi.org/10.1021/cm200782z>.
- [30] M. Reehuis, W. Jeitschko, Structure and magnetic properties of the phosphides CaCo₂P₂ and LnT₂P₂ with ThCr₂Si₂ structure and LnTP with PbFCl structure (Ln = Lanthanoids,

- T = Fe, Co, Ni)[†], *J. Phys. Chem. Solids.* 51 (1990) 961–968. [https://doi.org/10.1016/0022-3697\(90\)90039-I](https://doi.org/10.1016/0022-3697(90)90039-I).
- [31] P.A. Joy, P.S.A. Kumar, S.K. Date, The relationship between field-cooled and zero-field-cooled susceptibilities of some ordered magnetic systems, *J. Phys. Condens. Matter.* 10 (1998) 11049–11054. <https://doi.org/10.1088/0953-8984/10/48/024>.

Supplementary Information

Theory-guided Investigation on Magnetic Evolution of $\text{MnPt}_{5-x}\text{Pd}_x\text{P}$ and Discovery of anti-CeCoIn₅-type Ferromagnetic MnPd_5P

Ranuri S. Dissanayaka Mudiyansele,¹ Chang-Jong Kang,^{2,3} Kaya Wei,⁴ Zhixue Shu⁵, Tai Kong⁵, Ryan Baumbach,⁴ Gabriel Kotliar,² Weiwei Xie^{1*}

¹Department of Chemistry and Chemical Biology, Rutgers University, Piscataway, NJ, 08854, USA

²Department of Physics and Astronomy, Rutgers University, Piscataway, NJ, 08854, USA

³Department of Physics, Chungnam National University, Daejeon, 34134, South Korea

⁴National High Magnetic Field Laboratory, Tallahassee, FL, 32310, USA

⁵Department of Physics, University of Arizona, Tucson, AZ 85721, USA

Table of Contents

Table S1. Single crystal structure refinement for $\text{MnPt}_{5-x}\text{Pd}_x\text{P}$	19
Table. S2. Atomic distributions for $\text{MnPt}_{5-x}\text{Pd}_x\text{P}$	20
Figure S1. Refined powder diffraction pattern of MnPd_5P	21
Table S3. The percentages of impurities for $\text{MnPt}_{5-x}\text{Pd}_x\text{P}$	22
Table S4. Chemical compositions obtained from SEM-EDX.....	23
Figure S2. Comparison of magnetic susceptibility vs T	25
Figure S3. Summary of magnetic parameters derived from Curie-Weiss fitting.....	26

Table S1. Single crystal structure refinement for MnPt_{5-x}PdP at 300 (2) K. (Standard deviation is indicated by the values in parentheses)

Loaded composition	MnPd ₅ P	MnPd ₄ PtP	MnPd ₃ Pt ₂ P	MnPd _{2.5} Pt _{2.5} P	MnPd ₂ Pt ₃ P	MnPdPt ₄ P
Refined Formula	MnPd ₅ P	MnPd _{4.14(2)} Pt _{0.86(2)} P	MnPd _{2.73} Pt _{2.27} P	MnPd _{2.4} Pt _{2.6} P	MnPd _{2.10} Pt _{2.90} P	
F.W. (g/mol)	617.91	694.18	819.24	848.50	875.11	
Space group; Z	<i>P</i> 4/ <i>mmm</i> ; 1	<i>P</i> 4/ <i>mmm</i> ; 1	<i>P</i> 4/ <i>mmm</i> ; 1	<i>P</i> 4/ <i>mmm</i> ; 1	<i>P</i> 4/ <i>mmm</i> ; 1	
<i>a</i> (Å)	3.899 (2)	3.894 (1)	3.887 (2)	3.888 (2)	3.901 (3)	3.902(2)
<i>c</i> (Å)	6.867 (4)	6.855 (1)	6.853 (2)	6.861 (2)	6.892 (4)	6.921(3)
V (Å ³)	104.42 (2)	103.93 (2)	103.54 (4)	103.73 (5)	104.93 (11)	105.41 (7)
θ range (°)	2.966-34.770	5.236-34.828	5.246-34.892	2.969-3.874	5.919-34.646	
No. reflections; <i>R</i> _{int}	578; 0.0609	1397; 0.0293	999; 0.0444	904; 0.0549	214; 0.0233	
No. independent reflections	170	173	166	167	94	
No. parameters	12	14	14	14	14	
<i>R</i> ₁ ; ω <i>R</i> ₂ (<i>I</i> >2σ(<i>I</i>))	0.0509; 0.1204	0.0253; 0.0603	0.0429; 0.1026	0.0417; 0.1080	0.0373; 0.0947	
Goodness of fit	1.282	1.346	1.331	1.429	1.154	
Diffraction peak and hole (e ⁻ / Å ³)	2.656; -1.863	2.632; -1.926	7.771; -3.765	7.323; 5.219	2.579; -3.540	
Temperature	300 (2)	299 (2)	301 (2)	300 (2)	301 (2)	

Table S2. Atomic coordinates, occupancies and equivalent isotropic displacement parameters of $\text{MnPt}_{5-x}\text{PdP}$ at 300 (2) K. (U_{eq} is defined as one-third of the trace of the orthogonalized U_{ij} tensor (\AA^2)).

Atom	Wyckoff.	Occ.	x	y	z	U_{eq}
MnPd5P						
Pd1	$4i$	1	0	$\frac{1}{2}$	0.2948 (1)	0.015(1)
Pd2	$1a$	1	0	0	0	0.012(2)
Mn3	$1c$	1	$\frac{1}{2}$	$\frac{1}{2}$	0	0.022(1)
P4	$1b$	1	0	0	$\frac{1}{2}$	0.016(2)
MnPd₄PtP						
Pd1	$4i$	0.84(2)	0	$\frac{1}{2}$	0.29385(9)	0.0058(2)
Pt2	$4i$	0.22(2)	0	$\frac{1}{2}$	0.2948 (1)	0.0058(2)
Pd3	$1a$	0.78(2)	0	0	0	0.0046(3)
Pt4	$1a$	0.22(2)	0	0	0	0.0046(3)
Mn3	$1c$	1	$\frac{1}{2}$	$\frac{1}{2}$	0	0.0128(9)
P4	$1b$	1	0	0	$\frac{1}{2}$	0.0076(11)
MnPd₃Pt₂P						
Pd1	$4i$	0.57(6)	0	$\frac{1}{2}$	0.29296(17)	0.0056(4)
Pt2	$4i$	0.43 (6)	0	$\frac{1}{2}$	0.29296(17)	0.0056(4)
Pd3	$1a$	0.55(6)	0	0	0	0.0037(6)
Pt4	$1a$	0.45(6)	0	0	0	0.0037(6)
Mn3	$1c$	1	$\frac{1}{2}$	$\frac{1}{2}$	0	0.020(2)
P4	$1b$	1	0	0	$\frac{1}{2}$	0.006(2)
MnPd_{2.5}Pt_{2.5}P						
Pd1	$4i$	0.50(8)	0	$\frac{1}{2}$	0.29274(18)	0.0078(5)
Pt2	$4i$	0.50 (8)	0	$\frac{1}{2}$	0.29274(18)	0.0078(5)
Pd3	$1a$	0.42(6)	0	0	0	0.0049(7)
Pt4	$1a$	0.58(6)	0	0	0	0.0049(7)
Mn3	$1c$	1	$\frac{1}{2}$	$\frac{1}{2}$	0	0.015(3)
P4	$1b$	1	0	0	$\frac{1}{2}$	0.011(3)
MnPd₂Pt₃P						
Pd1	$4i$	0.43(6)	0	$\frac{1}{2}$	0.29254(11)	0.0084(6)
Pt2	$4i$	0.57 (6)	0	$\frac{1}{2}$	0.29254(11)	0.0084(6)
Pd3	$1a$	0.38(6)	0	0	0	0.0068(7)
Pt4	$1a$	0.62(6)	0	0	0	0.0068(7)
Mn3	$1c$	1	$\frac{1}{2}$	$\frac{1}{2}$	0	0.012(3)
P4	$1b$	1	0	0	$\frac{1}{2}$	0.014(4)

Figure S1. Powder diffraction pattern of MnPd₅P. The red, black and blue solid line represent experimental data (I_{obs}), the calculated LeBail refinement (I_{cal}) and the difference between calculated and observed intensities ($I_{\text{obs}} - I_{\text{cal}}$), respectively. The green vertical bars mark the expected Bragg positions for MnPd₅P.

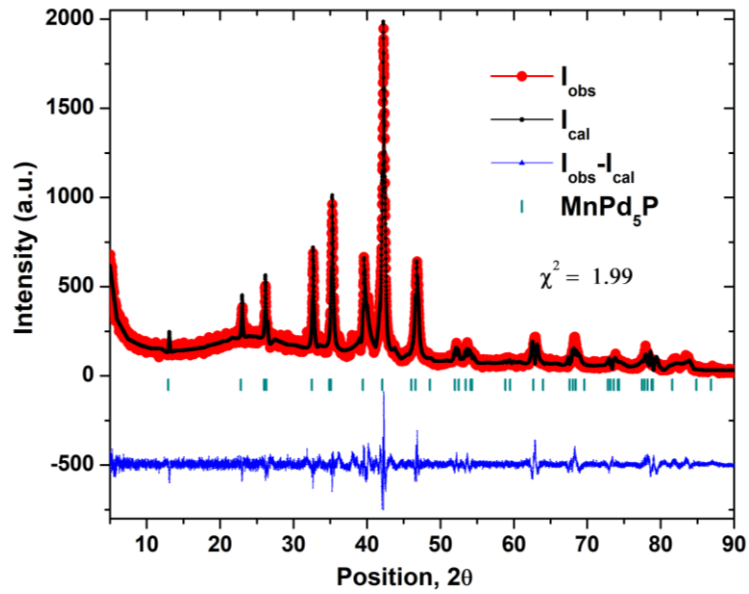


Table S3. The percentages of impurities determined from the Rietveld refinement in the HighScore Plus software for $\text{MnPt}_{5-x}\text{Pd}_x\text{P}$.

	$\text{MnPt}_{5-x}\text{Pd}_x\text{P}$ %	PdPt %	MnPdP %	Pt %	MnPt %
MnPd_4PtP	86.8	9.8	3.1	0.3	0
$\text{MnPd}_3\text{Pt}_2\text{P}$	82.7	14.4	3.2	1.7	0.6
$\text{MnPd}_{2.5}\text{Pt}_{2.5}\text{P}$	51.2	15.4	32	1.4	0
$\text{MnPd}_2\text{Pt}_3\text{P}$	75.8	19.1	4.1	1.0	0
MnPdPt_4P	93.1	2.0	1.5	3.3	0

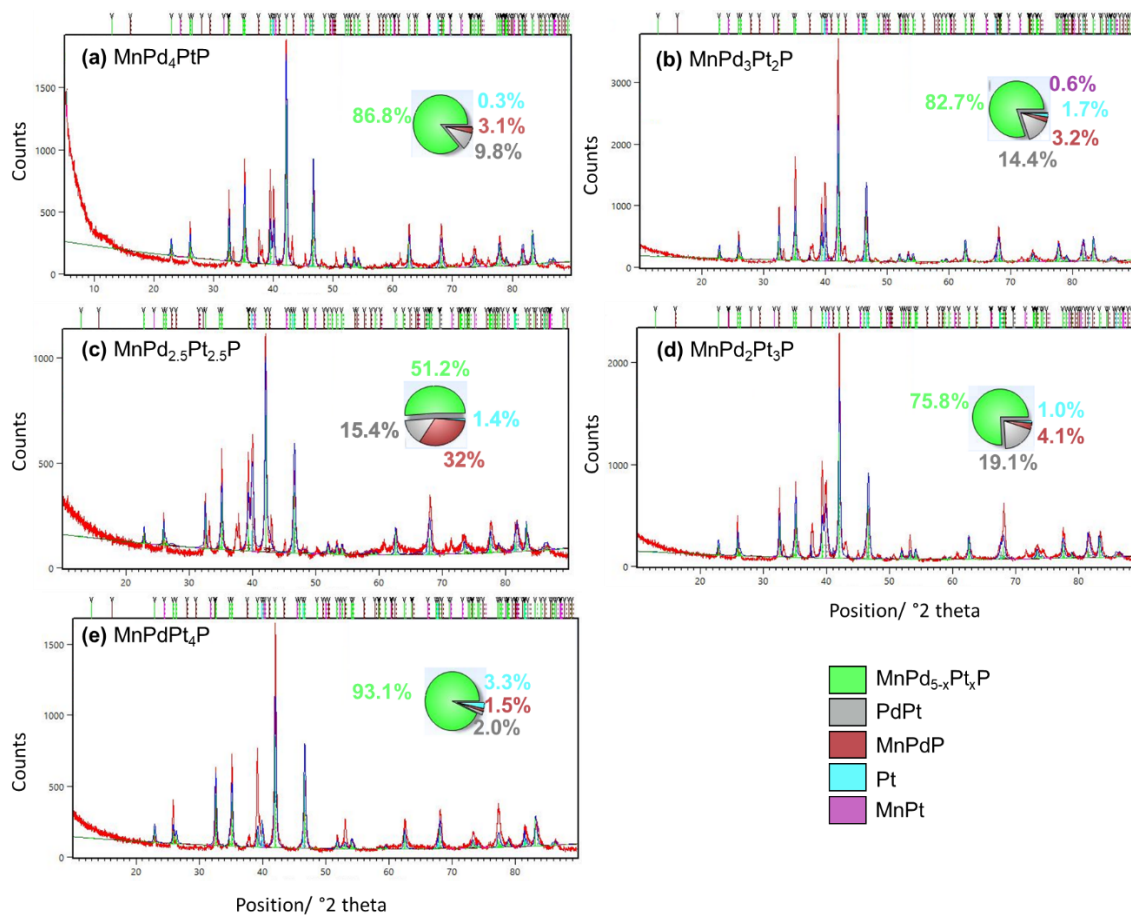
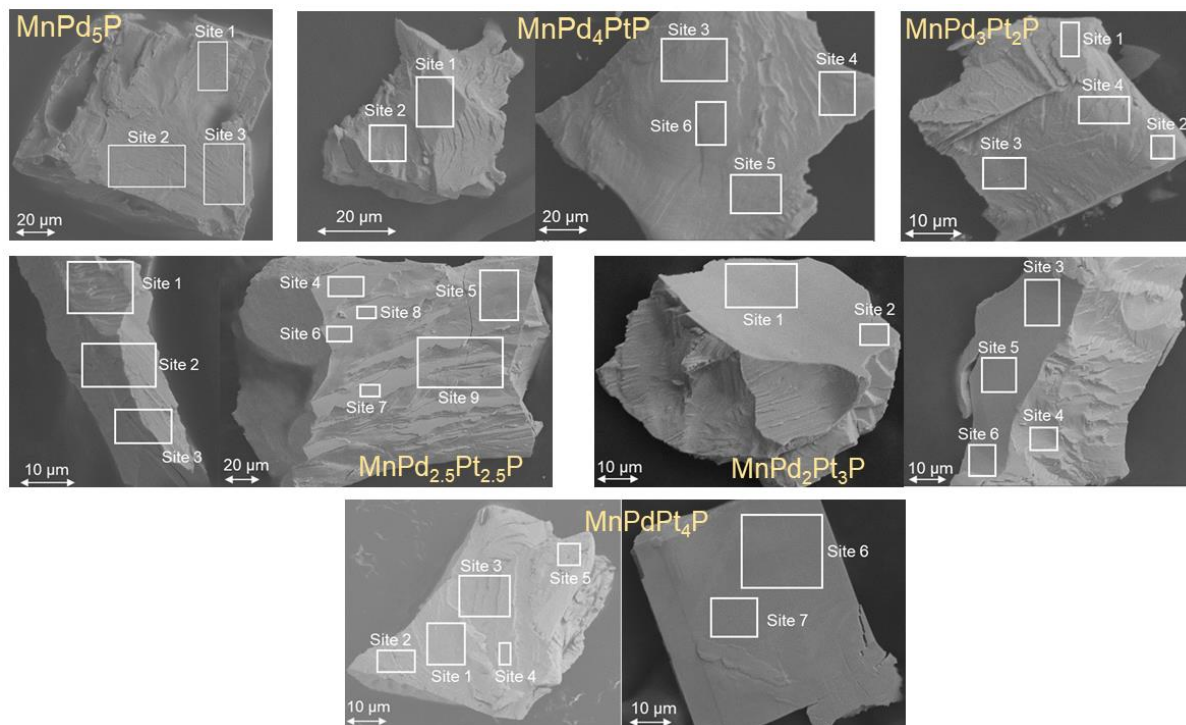


Table S4. Chemical compositions obtained from SEM-EDX for the loaded $\text{MnPt}_{5-x}\text{Pd}_x\text{P}$ samples and the corresponding crystal images



MnPd₅P						
		<i>Mn</i>	<i>Pd</i>	<i>P</i>		<i>Composition</i>
<i>Crystal-1</i>	<i>Site1</i>	14.95	72.34	12.71		$\text{Mn}_{1.00}\text{Pd}_{4.84}\text{P}_{0.85}$
						$\text{Mn}_{1.05}\text{Pd}_{5.06}\text{P}_{0.89}$
						$\text{Mn}_{1.06}\text{Pd}_{5.09}\text{P}_{0.85}$
						$\text{Mn}_{1.12}\text{Pd}_{5.10}\text{P}_{0.81}$
						$\text{Mn}_{1.07}\text{Pd}_{5.08}\text{P}_{0.85}$
	<i>Site2</i>	15.10	72.78	12.12		$\text{Mn}_{1.00}\text{Pd}_{4.82}\text{P}_{0.80}$
	<i>Site3</i>	15.95	72.38	11.67		$\text{Mn}_{1.00}\text{Pd}_{4.54}\text{P}_{0.73}$
					<i>Average</i>	$\text{Mn}_{1.00}\text{Pd}_{4.73}\text{P}_{0.79}$
MnPd₄PtP						
		<i>Mn</i>	<i>Pd</i>	<i>Pt</i>	<i>P</i>	<i>Composition</i>
<i>Crystal-1</i>	<i>Site1</i>	14.60	59.07	13.03	13.29	$\text{Mn}_{1.00}\text{Pd}_{4.05}\text{Pt}_{0.89}\text{P}_{0.91}$
	<i>Site2</i>	17.5	57.00	12.91	12.59	$\text{Mn}_{1.00}\text{Pd}_{3.26}\text{Pt}_{0.74}\text{P}_{0.72}$
<i>Crystal-2</i>	<i>Site3</i>	13.99	58.20	15.12	12.68	$\text{Mn}_{1.00}\text{Pd}_{4.16}\text{Pt}_{1.08}\text{P}_{0.91}$
	<i>Site4</i>	13.95	60.65	12.99	12.40	$\text{Mn}_{1.00}\text{Pd}_{4.35}\text{Pt}_{0.93}\text{P}_{0.89}$
	<i>Site5</i>	14.33	58.28	14.96	12.43	$\text{Mn}_{1.00}\text{Pd}_{4.07}\text{Pt}_{1.04}\text{P}_{0.87}$
	<i>Site6</i>	14.01	57.14	15.14	13.47	$\text{Mn}_{1.00}\text{Pd}_{4.08}\text{Pt}_{1.08}\text{P}_{0.96}$
					<i>Average</i>	$\text{Mn}_{1.00}\text{Pd}_{3.99}\text{Pt}_{0.96}\text{P}_{0.88}$
MnPd₃Pt₂P						
		<i>Mn</i>	<i>Pd</i>	<i>Pt</i>	<i>P</i>	<i>Composition</i>

<i>Crystal-1</i>	<i>Site1</i>	15.09	42.82	29.91	12.18	$\text{Mn}_{1.00}\text{Pd}_{2.84}\text{Pt}_{1.98}\text{P}_{0.81}$
	<i>Site2</i>	15.14	41.98	29.98	12.63	$\text{Mn}_{1.00}\text{Pd}_{2.77}\text{Pt}_{1.98}\text{P}_{0.83}$
	<i>Site3</i>	14.01	43.74	30.04	12.21	$\text{Mn}_{1.00}\text{Pd}_{3.12}\text{Pt}_{2.14}\text{P}_{0.87}$
	<i>Site4</i>	15.35	42.50	29.44	12.71	$\text{Mn}_{1.00}\text{Pd}_{2.77}\text{Pt}_{1.92}\text{P}_{0.83}$
Average						$\text{Mn}_{1.00}\text{Pd}_{2.88}\text{Pt}_{2.01}\text{P}_{0.84}$
MnPd_{2.5}Pt_{2.5}P						
		<i>Mn</i>	<i>Pd</i>	<i>Pt</i>	<i>P</i>	<i>Composition</i>
<i>Crystal-1</i>	<i>Site1</i>	13.81	37.78	36.89	11.53	$\text{Mn}_{1.00}\text{Pd}_{2.74}\text{Pt}_{2.67}\text{P}_{0.83}$
	<i>Site2</i>	14.08	37.44	35.78	12.69	$\text{Mn}_{1.00}\text{Pd}_{2.66}\text{Pt}_{2.54}\text{P}_{0.90}$
	<i>Site3</i>	14.71	37.31	35.94	12.04	$\text{Mn}_{1.00}\text{Pd}_{2.54}\text{Pt}_{2.44}\text{P}_{0.82}$
<i>Crystal-2</i>	<i>Site4</i>	15.50	35.99	36.54	11.98	$\text{Mn}_{1.00}\text{Pd}_{2.32}\text{Pt}_{2.36}\text{P}_{0.77}$
	<i>Site5</i>	13.83	37.42	36.72	12.03	$\text{Mn}_{1.00}\text{Pd}_{2.71}\text{Pt}_{2.66}\text{P}_{0.87}$
	<i>Site6</i>	16.11	35.40	35.96	12.53	$\text{Mn}_{1.00}\text{Pd}_{2.20}\text{Pt}_{2.23}\text{P}_{0.78}$
	<i>Site7</i>	15.53	35.99	36.56	11.93	$\text{Mn}_{1.00}\text{Pd}_{2.32}\text{Pt}_{2.35}\text{P}_{0.77}$
	<i>Site8</i>	15.26	35.97	36.37	12.40	$\text{Mn}_{1.00}\text{Pd}_{2.36}\text{Pt}_{2.38}\text{P}_{0.81}$
	<i>Site9</i>	14.44	36.41	36.50	12.65	$\text{Mn}_{1.00}\text{Pd}_{2.52}\text{Pt}_{2.53}\text{P}_{0.88}$
Average						$\text{Mn}_{1.00}\text{Pd}_{2.48}\text{Pt}_{2.46}\text{P}_{0.83}$
MnPd₂Pt₃P						
		<i>Mn</i>	<i>Pd</i>	<i>Pt</i>	<i>P</i>	<i>Composition</i>
<i>Crystal-1</i>	<i>Site1</i>	16.37	28.07	44.39	11.17	$\text{Mn}_{1.00}\text{Pd}_{1.71}\text{Pt}_{2.71}\text{P}_{0.68}$
	<i>Site2</i>	21.27	25.30	42.46	10.97	$\text{Mn}_{1.00}\text{Pd}_{1.19}\text{Pt}_{2.00}\text{P}_{0.52}$
<i>Crystal-2</i>	<i>Site3</i>	13.07	30.26	44.22	12.45	$\text{Mn}_{1.00}\text{Pd}_{2.32}\text{Pt}_{3.38}\text{P}_{0.95}$
	<i>Site4</i>	17.42	25.70	44.62	12.26	$\text{Mn}_{1.00}\text{Pd}_{1.48}\text{Pt}_{2.56}\text{P}_{0.70}$
	<i>Site5</i>	13.56	30.28	44.25	11.90	$\text{Mn}_{1.00}\text{Pd}_{2.23}\text{Pt}_{3.26}\text{P}_{0.88}$
	<i>Site6</i>	14.47	28.73	43.53	13.27	$\text{Mn}_{1.00}\text{Pd}_{1.99}\text{Pt}_{3.01}\text{P}_{0.92}$
Average						$\text{Mn}_{1.00}\text{Pd}_{1.82}\text{Pt}_{2.82}\text{P}_{0.78}$
MnPdPt₄P						
		<i>Mn</i>	<i>Pd</i>	<i>Pt</i>	<i>P</i>	<i>Composition</i>
<i>Crystal-1</i>	<i>Site1</i>	14.30	13.88	58.83	13.00	$\text{Mn}_{1.00}\text{Pd}_{0.97}\text{Pt}_{4.11}\text{P}_{0.91}$
	<i>Site2</i>	15.39	13.70	58.72	12.18	$\text{Mn}_{1.00}\text{Pd}_{0.89}\text{Pt}_{3.81}\text{P}_{0.79}$
	<i>Site3</i>	14.22	14.11	58.93	12.75	$\text{Mn}_{1.00}\text{Pd}_{0.99}\text{Pt}_{4.15}\text{P}_{0.90}$
	<i>Site4</i>	14.56	14.96	59.22	11.26	$\text{Mn}_{1.00}\text{Pd}_{0.97}\text{Pt}_{4.11}\text{P}_{0.91}$
	<i>Site5</i>	15.61	13.82	58.83	11.75	$\text{Mn}_{1.00}\text{Pd}_{0.88}\text{Pt}_{3.77}\text{P}_{0.76}$
<i>Crystal-3</i>	<i>Site6</i>	16.32	12.93	59.75	11.0	$\text{Mn}_{1.00}\text{Pd}_{0.79}\text{Pt}_{3.66}\text{P}_{0.67}$
	<i>Site7</i>	14.59	13.77	59.95	11.69	$\text{Mn}_{1.00}\text{Pd}_{0.94}\text{Pt}_{4.11}\text{P}_{0.80}$
Average						$\text{Mn}_{1.00}\text{Pd}_{0.92}\text{Pt}_{3.96}\text{P}_{0.82}$

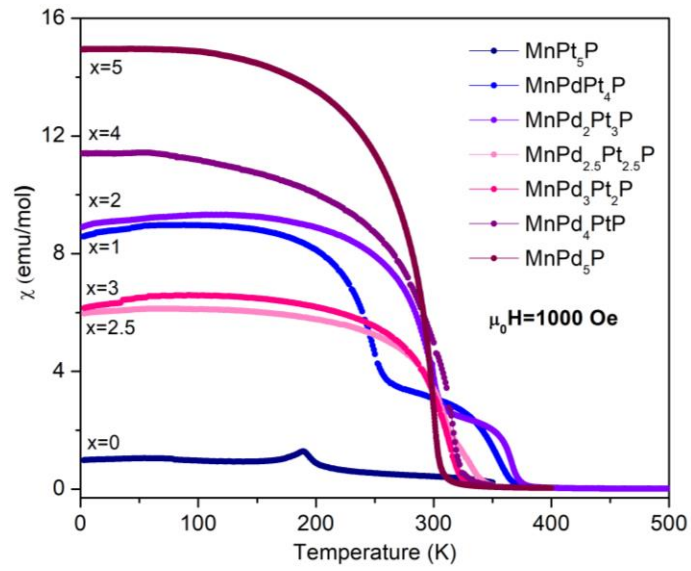
Figure S2. Comparison of magnetic susceptibility vs T for each compound at 1000 Oe

Figure S3. Summary of magnetic parameters derived from Curie-Weiss fitting

	MnPd ₅ P	MnPd ₄ PtP	MnPd ₃ Pt ₂ P	MnPd _{2.5} Pt _{2.5} P	MnPd ₂ Pt ₃ P	MnPdPt ₄ P
θ_{CW} (K)	304.4(1)	317.8(3)	318.0(1)	334.1(2)	369.9(1)	366.2(3)
C	3.13(1)	4.14(6)	2.45(1)	2.09(4)	1.09(1)	1.16(1)
μ_{eff} (μ_B)	5.00	5.75	4.43	4.09	2.95	3.04
R ²	0.999	0.992	0.999	0.989	0.998	0.989

